

Effect of Off-diagonal NSI Parameters on Entanglement Measurements in Neutrino Oscillations

Lekhashri Konwar,^{1,*} Papia Panda,^{2,†} and Rukmani Mohanta^{2,‡}

¹*Indian Institute of Technology Jodhpur, Jodhpur 342030, India*

²*School of Physics, University of Hyderabad, Hyderabad - 500046, India*

Abstract

In this work, we explore the influence of off-diagonal non-standard interaction (NSI) parameters on quantum entanglement within the three-flavor neutrino oscillation framework. By expressing three key entanglement measures: Entanglement of Formation (EOF), Concurrence, and Negativity in terms of oscillation probabilities, we analyze how these quantum correlations are affected by the NSI parameters $\epsilon_{e\mu}$, $\epsilon_{e\tau}$, and $\epsilon_{\mu\tau}$, including their complex phases. Using the DUNE experiment as a benchmark, we find that NSI effects are most significant at low energies, with Negativity showing the highest sensitivity even at high energies. It is observed that $\epsilon_{e\mu}$ and $\epsilon_{e\tau}$ affect entanglement measures mainly through the appearance channel, while the impact of $\epsilon_{\mu\tau}$ on EOF, Concurrence, and Negativity is predominantly linked to the disappearance channel.

* konwar.3@iitj.ac.in

† ppapia93@gmail.com

‡ rmisp@uohyd.ac.in

I. INTRODUCTION

Neutrino oscillation [1, 2] is a quantum mechanical phenomenon that arises from the mixing between neutrino flavor and mass eigenstates. Since neutrino flavor states are quantum superpositions of mass eigenstates, a neutrino originated with a specific flavor can be detected as a different flavor during propagation. The probabilities of such oscillations are governed by six key parameters: three mixing angles ($\theta_{12}, \theta_{13}, \theta_{23}$), two mass-squared differences ($\Delta m_{21}^2, \Delta m_{31}^2$), and a CP-violating phase, δ_{CP} . Over the past few decades, a broad range of solar, atmospheric, reactor, and accelerator neutrino experiments have measured most of these parameters with remarkable precision. Despite this progress, several fundamental questions remain unresolved, most notably are the ordering of neutrino masses, commonly known as mass hierarchy problem, the exact value of the CP-violating phase δ_{CP} , and whether the atmospheric mixing angle θ_{23} lies in the lower or upper octant. Addressing these unknowns is a primary goal of upcoming and ongoing high-precision neutrino oscillation experiments [3–6], which are designed not only to rigorously test the three-flavor paradigm but also to search for signatures of physics Beyond the Standard Model (BSM) [7–14].

Neutrino Physics has now entered the precision era, and at this point, it is crucial to study the sub-leading effects in neutrino oscillations, commonly termed as Non-Standard neutrino Interactions (NSIs), which introduce new coupling parameters to the theory, and thus play a pivotal role on the determination of unknowns in neutrino sector. A model-independent framework for exploring NSI effects in neutrino oscillations is discussed in Refs.[15–17]. Among the various possible new physics effects in the neutrino sector, NSIs have received significant attention and effectively modify neutrino production, detection, and most significantly propagation of neutrinos through matter [18]. These interactions can be described by dimension-six four-fermion operators, which introduce additional terms into the neutrino evolution Hamiltonian. In this work, we focus on propagation NSI, as constraints on production and detection NSI are typically more stringent. The matter NSI terms are parametrized by dimensionless coefficients $\epsilon_{\alpha\beta}$ ($\alpha, \beta = e, \mu, \tau$) that modify the effective matter potential experienced by neutrinos in propagation. These include both diagonal (flavor-conserving) and off-diagonal (flavor-violating) components, where the off-diagonal terms can be complex and introduce new CP-violating effects. Since NSIs affect the coherent forward scattering of neutrinos with electrons and quarks in matter, they can lead to significant modifications in oscillation probabilities, especially in long-baseline experiments with specific beamlines and detector setups [19–29].

Recent developments in quantum information theory have opened a novel and exciting perspective in the neutrino system [30–45]. Specifically, the concept of quantum entanglement, once considered relevant primarily in systems like atomic and optical systems, is now being investigated in the context of fundamental particles, including neutrinos [43, 46–50]. Entanglement represents a core feature of quantum mechanics, characterising non-classical

correlations between different components of a system [51]. In neutrino physics, the coherent superposition of mass and flavor eigenstates naturally leads to a form of single-particle mode entanglement [46, 52], where the different flavor modes of a single neutrino become quantum-mechanically correlated. The key insight is that these entanglement measures can be quantified using neutrino oscillation probabilities, which are directly measurable in neutrino oscillation experiments. To quantify entanglement in neutrino systems, several well-established measures from quantum information theory are employed. In this work, we focus on three such measures: entanglement of Formation (EOF) [53, 54], Concurrence [55–57] and Negativity [58–60].

Among the various entanglement measures, the EOF plays a prominent role and captures the minimum average entanglement over all pure state decompositions of a mixed state. Concurrence, initially formulated for bipartite qubit systems, has been successfully extended to tripartite scenarios and provides a robust way to evaluate the degree of entanglement through the reduced density matrices. Another widely used measure is negativity, which is derived from the Peres-Horodecki criterion [58]. It quantifies entanglement based on the partial transpose of the density matrix, acquiring negative eigenvalues, which serves as a clear signature of non-separability and, consequently, the presence of entanglement in the system. All three measures can be effectively expressed in terms of flavor transition probabilities, allowing the entanglement to be quantified using experimentally observable quantities and providing a framework to study quantum correlations in neutrino oscillations. In this study, we explore the behavior of three key entanglement measures within the framework of three-flavor neutrino oscillations by formulating them in terms of oscillation probabilities. We further examine how these measures are influenced by the presence of three complex off diagonal NSI scenarios.

The paper is organized as follows. Section II presents the theoretical formalism underlying neutrino oscillation with NSI, along with a description of mode entanglement in the three-flavor neutrino system. In Section III, we define the three entanglement measures used in our analysis: EOF, Concurrence and Negativity, and express them in terms of neutrino oscillation probabilities. Section IV discusses the simulation setup based on the DUNE experiment. Section V emphasizes the major results coming out from our work. Finally, Section VI summarizes the conclusions of the study.

II. FORMALISM

Neutrino oscillations arise as a consequence of both neutrino mixing and non-degenerate neutrino masses. The neutrino mass eigenstates $|\nu_j\rangle, j = 1, 2, 3$, associated with definite masses m_j and energies E_j , evolve in time of the form:

$$|\nu_j(t)\rangle = e^{-iE_j t} |\nu_j\rangle. \quad (1)$$

The flavor eigenstates $|\nu_\alpha\rangle$, $\alpha = e, \mu, \tau$ are linear superpositions of the mass eigenstates, and their time evolution is governed by the unitary operator $U_f(t)$, such that

$$|\nu_\alpha(t)\rangle = U_f(t) |\nu_\beta\rangle, \quad (2)$$

where $U_f(t) = Ue^{-iH_mt}U^{-1}$ is the time-evolution operator with $\mathcal{H}_m = \text{diag}(E_1, E_2, E_3)$ and U representing the PMNS matrix that relates the flavor and mass eigenstates. The flavor state $|\nu_\alpha(t)\rangle$ at time t can then be expressed in terms of the flavor basis as:

$$|\nu_\alpha(t)\rangle = U_{\alpha e}(t) |\nu\rangle_e + U_{\alpha \mu}(t) |\nu\rangle_\mu + U_{\alpha \tau}(t) |\nu\rangle_\tau. \quad (3)$$

The transition probability for a neutrino of flavor α to be detected as a neutrino of flavor β at time t is given by:

$$P_{(\nu_\alpha \rightarrow \nu_\beta)}(t) = |\langle \nu_\beta | \nu_\alpha(t) \rangle|^2 = |U_{\alpha\beta}(t)|^2 \quad (4)$$

This probability depends on the energy differences $\Delta E_{jk} = E_j - E_k$ for $(j, k = 1, 2, 3)$ and the parameters of the mixing matrix. In the ultra-relativistic limit, we approximate as, $\Delta E_{jk} \simeq (\Delta m_{jk}^2/2E)$ with $\Delta m_{jk}^2 = m_j^2 - m_k^2$ and E is the neutrino energy, assuming all mass eigenstates share the same momentum p .

In the scenarios beyond the SM, neutrino propagation can be affected by NSI with matter, which introduce additional effective potentials modifying the flavor evolution Hamiltonian. The NSI formalism extends the standard oscillation framework by incorporating these new interactions as perturbations in the matter potential, typically parameterized by dimensionless coefficients $\epsilon_{\alpha\beta}$ with $\alpha, \beta = e, \mu, \tau$ [15, 16, 61]. This approach allows for a systematic study of how beyond-Standard-Model effects can influence neutrino oscillation probabilities.

In the relativistic limit, neutrino flavor states can be treated as distinguishable modes within a single-particle quantum field framework. When two or more of these modes exhibit non-factorizable quantum correlations, the system is said to possess mode entanglement. Specifically, neutrino mode entanglement refers to the entanglement among different flavor modes, such as electron, muon, and tau, within a single neutrino field. This type of entanglement arises naturally from the time evolution of flavor states due to neutrino mixing. As a result, a time-evolved neutrino flavor state can be interpreted as an entangled superposition across the flavor modes. For a three-flavor neutrino system, each flavor state can be formally represented in the occupation number basis as a three-qubit configuration [46]: $|\nu_e\rangle \equiv |1\rangle_e |0\rangle_\mu |0\rangle_\tau$, $|\nu_\mu\rangle \equiv |0\rangle_e |1\rangle_\mu |0\rangle_\tau$ and $|\nu_\tau\rangle \equiv |0\rangle_e |0\rangle_\mu |1\rangle_\tau$. Here, $|0\rangle_\alpha$ and $|1\rangle_\alpha$ denote the absence and presence, respectively, of a neutrino in the flavor mode ν_α . The general time-evolved state $|\nu_\alpha(t)\rangle$ (14) takes the form:

$$|\nu_\alpha(t)\rangle = U_{\alpha e}(t) |1\rangle_e |0\rangle_\mu |0\rangle_\tau + U_{\alpha \mu}(t) |0\rangle_e |1\rangle_\mu |0\rangle_\tau + U_{\alpha \tau}(t) |0\rangle_e |0\rangle_\mu |1\rangle_\tau. \quad (5)$$

Here, each term in this expression represents the occupation of one specific flavor mode (e , μ , or τ) while the others remain unoccupied.

To analyze this entanglement quantitatively, the density matrix of the system at time t is

constructed as, $\rho_{ABC}^\alpha(t) = |\nu_\alpha(t)\rangle \langle \nu_\alpha(t)|$. For the neutrino state, the density matrix takes the form [43]:

$$\rho_{ABC}^\alpha(t) = \begin{pmatrix} 0 & 0 & 0 & 0 & 0 & 0 & 0 & 0 \\ 0 & \rho_{22}^\alpha & \rho_{23}^\alpha & 0 & \rho_{25}^\alpha & 0 & 0 & 0 \\ 0 & \rho_{32}^\alpha & \rho_{33}^\alpha & 0 & \rho_{35}^\alpha & 0 & 0 & 0 \\ 0 & 0 & 0 & 0 & 0 & 0 & 0 & 0 \\ 0 & \rho_{52}^\alpha & \rho_{53}^\alpha & 0 & \rho_{55}^\alpha & 0 & 0 & 0 \\ 0 & 0 & 0 & 0 & 0 & 0 & 0 & 0 \\ 0 & 0 & 0 & 0 & 0 & 0 & 0 & 0 \\ 0 & 0 & 0 & 0 & 0 & 0 & 0 & 0 \end{pmatrix}, \quad (6)$$

where the elements of this matrix can be represented as.

$$\begin{aligned} \rho_{22}^\alpha &= |\bar{U}_{\alpha\tau}(t)|^2; & \rho_{23}^\alpha &= \bar{U}_{\alpha\tau}(t)\bar{U}_{\alpha\mu}^*(t); & \rho_{25}^\alpha &= \bar{U}_{\alpha\tau}(t)\bar{U}_{\alpha e}^*(t); \\ \rho_{32}^\alpha &= \bar{U}_{\alpha\mu}(t)\bar{U}_{\alpha\tau}^*(t); & \rho_{33}^\alpha &= |\bar{U}_{\alpha\mu}(t)|^2; & \rho_{35}^\alpha &= \bar{U}_{\alpha\mu}(t)\bar{U}_{\alpha e}^*(t); \\ \rho_{52}^\alpha &= \bar{U}_{\alpha e}(t)\bar{U}_{\alpha\tau}^*(t); & \rho_{53}^\alpha &= \bar{U}_{\alpha e}(t)\bar{U}_{\alpha\mu}^*(t); & \rho_{55}^\alpha &= |\bar{U}_{\alpha e}(t)|^2. \end{aligned} \quad (7)$$

The probabilities are as follows: $P_{\alpha e}(t) = |\bar{U}_{\alpha e}(t)|^2$, $P_{\alpha\mu}(t) = |\bar{U}_{\alpha\mu}(t)|^2$, and $P_{\alpha\tau}(t) = |\bar{U}_{\alpha\tau}(t)|^2$. In the next section, we will discuss the mathematical expressions of EOF, Concurrence and Negativity in three-flavor neutrino system.

III. ENTANGLEMENT MEASURES

A. Entanglement of Formation

In quantum mechanics, a pure state is said to be entangled if it cannot be written as a product of states of its subsystems. That is, the total state γ cannot be expressed as $\gamma_A \otimes \gamma_B$, then the state is entangled. A convenient way to measure this entanglement is through the entropy of entanglement, which is defined as the von Neumann entropy of either of the reduced density matrices: [53]

$$E(\gamma) = S(\rho_A) = S(\rho_B),$$

where $S(\rho) = -\text{Tr}(\rho \log_2 \rho)$ is the von Neumann entropy. The reduced density matrix ρ_A is obtained by tracing out subsystem B , $\rho_A = \text{Tr}_B(|\gamma\rangle \langle \gamma|)$, and vice versa for ρ_B .

When dealing with mixed states, entanglement can still be quantified using the EOF. For a mixed state, EOF, M is defined as the minimum average entanglement over all possible pure-state decompositions that realize M [53]:

$$E(M) = \min \sum_i p_i E(\gamma_i),$$

where $M = \sum_i p_i |\gamma_i\rangle \langle \gamma_i|$ and the minimization is over all possible sets of pure states $|\gamma_i\rangle$ and corresponding probabilities p_i that reproduce the mixed state M .

For a given pure state γ , EOF is computed to the entropy of entanglement:

$$EOF(\gamma) = -Tr(\rho_A \log_2 \rho_A) = -Tr(\rho_B \log_2 \rho_B), \quad (8)$$

where ρ_A and ρ_B are the reduced density matrices of the two subsystems. This definition can also be extended to tripartite systems. For a pure three-partite state $\rho_{ABC}(t)$, the EOF is given by [54]:

$$EOF(\rho_{ABC}(t)) = \frac{1}{2}[S(\rho_A) + S(\rho_B) + S(\rho_C)], \quad (9)$$

where $S(\rho_A)$, $S(\rho_B)$ and $S(\rho_C)$ are von Neumann entropies defined as $S(\rho_A) = -Tr(\rho_A \log \rho_A)$ and same with $S(\rho_B)$ and $S(\rho_C)$. ρ_A , ρ_B and ρ_C are reduced density matrices which have the expressions [54], $\rho_A = Tr_{BC}(\rho_{ABC}(t))$, $\rho_B = Tr_{AC}(\rho_{ABC}(t))$ and $\rho_C = Tr_{AB}(\rho_{ABC}(t))$.

The EOF for a neutrino initial flavor state, μ can be expressed in terms of the flavor transition probabilities as follows [62]:

$$EOF^\mu = -\frac{1}{2}[P_{\mu e} \log_2 P_{\mu e} + P_{\mu\mu} \log_2 P_{\mu\mu} + P_{\mu\tau} \log_2 P_{\mu\tau} + (P_{\mu\mu} + P_{\mu\tau}) \log_2 (P_{\mu\mu} + P_{\mu\tau}) + (P_{\mu e} + P_{\mu\tau}) \log_2 (P_{\mu e} + P_{\mu\tau}) + (P_{\mu\mu} + P_{\mu e}) \log_2 (P_{\mu\mu} + P_{\mu e})], \quad (10)$$

where $P_{\alpha\beta}$ are the oscillation probabilities from ν_α to ν_β transition.

B. Concurrence

For bipartite systems, particularly two-qubit systems, one of the most widely recognized and analytically tractable measures of entanglement is concurrence. Originally introduced by Hill and Wootters [55] and later generalized by Wootters [56], concurrence provides a quantification of the entanglement of formation for arbitrary mixed states of two qubits. However, a recent study has established that the framework of concurrence can be generalized to entanglement in three-qubit states, thereby extending its applicability beyond bipartite systems. This development constitutes a significant contribution to the theoretical understanding of entanglement in multipartite quantum systems, [57]

$$C(\rho_{ABC}) = [3 - Tr(\rho_A)^2 - Tr(\rho_B)^2 - Tr(\rho_C)^2]^{\frac{1}{2}}, \quad (11)$$

where ρ_A , ρ_B , and ρ_C are the reduced density matrices.

For oscillating neutrinos, the concurrence for vacuum can be expressed in terms of oscillation and survival probabilities as [62]

$$C^\mu = \sqrt{3 - 3P_S - 2P_{\mu\mu}P_{\mu\tau} - 2P_{\mu e}(P_{\mu\mu} + P_{\mu\tau})}, \quad (12)$$

where P_S is the sum of the square of probabilities, and defined as $(P_{\mu e}^2 + P_{\mu\mu}^2 + P_{\mu\tau}^2)$.

C. Negativity

A necessary condition for separability is provided by the Peres-Horodecki criterion [58], which states that the partial transpose of a separable state must have only non-negative eigenvalues. Violation of this condition implies that the state is entangled. Negativity is a computable entanglement measure based on this criterion. It is defined using the partial transpose ρ^{T_A} of the bipartite density matrix ρ with respect to subsystem A. Negativity quantifies how much ρ^{T_A} fails to be positive and is given by [59]:

$$N(\rho) = -2 \sum_i \sigma_i(\rho^{T_A}),$$

where $\sigma_i(\rho^{T_A})$ are the negative eigenvalues of the partial transpose ρ^{T_A} of the total state ρ with respect to the subsystem A. The negativity vanishes for separable states and provides a quantitative measure of the degree of entanglement present in composite quantum systems. The tripartite negativity of a state ρ_{ABC} is defined as [60]

$$N = (N_{A-BC} N_{B-CA} N_{C-AB})^{\frac{1}{3}},$$

with $N_{I-JK} = -2 \sum_i \sigma_i(\rho^{T_I})$ being the negative eigenvalues of ρ^{T_I} , the partial transpose of ρ with respect to subsystem I , with $I = A, B, C$, and $JK = BC, CA, AB$, respectively.

In terms of survival and oscillation probabilities of neutrino oscillation, negativity is given as [62] :

$$N^\mu = [\sqrt{P_{\mu e}} \sqrt{P_{\mu\mu} + P_{\mu\tau}} \sqrt{P_{\mu e} + P_{\mu\tau}} \sqrt{P_{\mu\mu}} \sqrt{P_{\mu e} + P_{\mu\mu}} \sqrt{P_{\mu\tau}}]^{\frac{1}{3}}. \quad (13)$$

IV. EXPERIMENTAL SETUP AND SIMULATION DETAILS

In this analysis, we consider the upcoming long-baseline neutrino experiment DUNE (Deep Underground Neutrino Experiment). DUNE is an ambitious forthcoming project featuring a baseline of 1300 km, extending from the Fermi National Accelerator Laboratory (FNAL) to the Sanford Underground Research Facility (SURF). For simulation purposes, we utilize the official configuration files based on the technical design report [63]. The experimental setup includes four liquid argon time-projection chamber (LArTPC) detectors, each with a mass of 10 kilotons, and operates with a 1.2 MW proton beam. The files represent an exposure of 624 kt-MW-years which corresponds to 6.5 years of run each in neutrino (FHC) and antineutrino (RHC) modes, using a 40 kt fiducial mass liquid argon time-projection chamber (LArTPC) far detector. For systematic errors, we use the numerical values from the ref. [63].

To perform the DUNE simulations, we employ the General Long-Baseline Experiment Simulator (GLOBES) framework [64, 65]. The probability engine within GLOBES has been

$\Delta m_{21}^2 (\text{eV}^2)$	$\Delta m_{31}^2 (\text{eV}^2)$	$\sin^2 \theta_{12}$	$\sin^2 \theta_{13}$	$\sin^2 \theta_{23}$	δ_{CP}
7.49×10^{-5}	2.513×10^{-3}	0.308	0.02215	0.470	212°

TABLE I: Best fit values of standard three-neutrino oscillation parameters used in our analysis [66].

NSI parameters	Best fit value
$ \epsilon_{e\mu} $	0.15
$ \epsilon_{e\tau} $	0.27
$ \epsilon_{\mu\tau} $	0.35
$\phi_{e\mu}$	1.38π rad
$\phi_{e\tau}$	1.62π rad
$\phi_{\mu\tau}$	0.6π rad

TABLE II: The best fit value of the NSI parameters used in the analysis [67, 68].

modified to incorporate the effects of non-standard interactions (NSI) in the neutrino oscillation probability calculations.

To estimate the sensitivities, we use the Poisson log-likelihood method, defined as

$$\chi^2 = 2 \sum_{i=1}^n \left[\mathcal{N}_i^{\text{test}} - \mathcal{N}_i^{\text{true}} - \mathcal{N}_i^{\text{true}} \log \left(\frac{\mathcal{N}_i^{\text{test}}}{\mathcal{N}_i^{\text{true}}} \right) \right], \quad (14)$$

where, $\mathcal{N}_i^{\text{true}}$ and $\mathcal{N}_i^{\text{test}}$ are the event numbers in the true and test spectra, respectively, and the index i runs over the energy bins. The true values of the oscillation parameters used in the analysis are taken from Ref. [69]. A marginalization over the relevant oscillation parameters is performed during the χ^2 analysis. In this work, we restrict our results to the normal mass ordering scenario, i.e., $\Delta m_{31}^2 > 0$.

V. RESULTS

In this section, we will illustrate the main results of our simulation. In the first subsection, we show how the appearance and disappearance probabilities are modified in the presence of off-diagonal NSI parameters, incorporating one parameter at a time. Then, in the following subsection, we discuss the effect of off-diagonal NSI parameters in the entanglement measures: EOF, Concurrence, and Negativity.

A. Analysis in probability level

In this subsection, we discuss how non-standard interaction (NSI) parameters influence the appearance and disappearance probabilities within the framework of the DUNE exper-

iment. At the source, a beam of muon neutrinos (ν_μ) is generated and travels through matter over a baseline of 1300 km to reach the far detector. Therefore, our primary focus is on the oscillation ($P_{\mu e}$) and survival ($P_{\mu\mu}$) probabilities. The presence of NSI modifies the standard probability expressions. In this analysis, we concentrate specifically on the off-diagonal NSI parameters: $\epsilon_{e\mu}$, $\epsilon_{e\tau}$, and $\epsilon_{\mu\tau}$. Since these are off-diagonal elements, they can possess both real and imaginary components, each associated with a corresponding phase: $\phi_{e\mu}$, $\phi_{e\tau}$, and $\phi_{\mu\tau}$. The appearance probability $P_{\mu e}$, modified by the presence of off-diagonal NSI parameters, can be expressed as follows ¹ [61]:

$$\begin{aligned}
P(\nu_\mu \rightarrow \nu_e) = & x^2 f^2 + 2xyfg \cos(\Delta + \delta_{CP}) + y^2 g^2 \\
& + 4\hat{A}\epsilon_{e\mu} \left\{ xf[s_{23}^2 f \cos(\phi_{e\mu} + \delta_{CP}) + c_{23}^2 g \cos(\Delta + \delta_{CP} + \phi_{e\mu})] \right. \\
& + yg[c_{23}^2 g \cos \phi_{e\mu} + s_{23}^2 f \cos(\Delta - \phi_{e\mu})] \left. \right\} \\
& + 4\hat{A}\epsilon_{e\tau} s_{23} c_{23} \left\{ xf[f \cos(\phi_{e\tau} + \delta_{CP}) - g \cos(\Delta + \delta_{CP} + \phi_{e\tau})] \right. \\
& - yg[g \cos \phi_{e\tau} - f \cos(\Delta - \phi_{e\tau})] \left. \right\} \\
& + 4\hat{A}^2 \left(g^2 c_{23}^2 |c_{23}\epsilon_{e\mu} - s_{23}\epsilon_{e\tau}|^2 + f^2 s_{23}^2 |s_{23}\epsilon_{e\mu} + c_{23}\epsilon_{e\tau}|^2 \right) \\
& + 8\hat{A}^2 fg s_{23} c_{23} \left\{ c_{23} \cos \Delta [s_{23}(\epsilon_{e\mu}^2 - \epsilon_{e\tau}^2) + 2c_{23}\epsilon_{e\mu}\epsilon_{e\tau} \cos(\phi_{e\mu} - \phi_{e\tau})] \right. \\
& - \epsilon_{e\mu}\epsilon_{e\tau} \cos(\Delta - \phi_{e\mu} + \phi_{e\tau}) \left. \right\} + \mathcal{O}(s_{13}\epsilon, s_{13}\epsilon^2, \epsilon^3), \tag{15}
\end{aligned}$$

where,

$$\begin{aligned}
x &\equiv 2s_{13}s_{23}, \quad y \equiv 2\alpha s_{12}c_{12}c_{23}, \quad \alpha = \frac{\Delta m_{21}^2}{\Delta m_{31}^2}, \\
f &\equiv \frac{\sin[\Delta(1 - \hat{A})]}{(1 - \hat{A})}, \quad g \equiv \frac{\sin(\hat{A}\Delta)}{\hat{A}}, \\
\Delta &= \frac{\Delta m_{31}^2 L}{4E}, \quad \hat{A} = \frac{A}{\Delta m_{31}^2}, \tag{16}
\end{aligned}$$

for normal ordering. For the inverted mass ordering, the corresponding substitutions are: $\Delta \rightarrow -\Delta$, $y \rightarrow -y$ and $\hat{A} \rightarrow -\hat{A}$. In the case of antineutrinos, Eq. 15 is modified by the following transformations: $\hat{A} \rightarrow -\hat{A}$, $\delta_{CP} \rightarrow -\delta_{CP}$ and $\phi_{\alpha\beta} \rightarrow -\phi_{\alpha\beta}$. Here $c_{ij} = \cos \theta_{ij}$, $s_{ij} = \sin \theta_{ij}$ with $i, j = 1, 2, 3$ and $A = 2\sqrt{2}G_F N_e E$, is the standard matter potential. G_F is the Fermi constant and N_e is the electron number density. From Eq. 15, it is evident that $P_{\mu e}$ largely depends on the off-diagonal NSI parameters $\epsilon_{e\mu}$, $\epsilon_{e\tau}$ and their associated phases, while it remains nearly independent of $\epsilon_{\mu\tau}$ (however, at subleading order, a dependence on $\epsilon_{\mu\tau}$ does appear).

¹ In Ref. [61], the expression for $P_{\mu e}$ also includes contributions from diagonal NSI terms (such as ϵ_{ee}). However, since our analysis focuses exclusively on the off-diagonal parameters, Eq. 15 is formulated solely in terms of these off-diagonal contributions, keeping $\epsilon_{ee} = 0$.

The disappearance probability in presence of off-diagonal NSI parameters can be written as ² [61]:

$$\begin{aligned}
P(\nu_\mu \rightarrow \nu_\mu) = & 1 - \sin^2 2\theta_{23} \sin^2 \Delta + \alpha c_{12}^2 \sin^2 2\theta_{23} \Delta \sin 2\Delta - \frac{4s_{23}^4 s_{13}^2 \sin^2(1 - \hat{A})\Delta}{(1 - \hat{A})^2} \\
& - \frac{\sin^2 2\theta_{23} s_{13}^2}{(1 - \hat{A})^2} \left[\hat{A}(1 - \hat{A})\Delta \sin 2\Delta + \sin(1 - \hat{A})\Delta \sin(1 + \hat{A})\Delta \right] \\
& - 2\hat{A}\epsilon_{\mu\tau} \cos \phi_{\mu\tau} \left[\sin^3 2\theta_{23} \Delta \sin 2\Delta + 2 \sin 2\theta_{23} \cos^2 2\theta_{23} \sin^2 \Delta \right] \\
& - 2\hat{A}^2 \sin^2 2\theta_{23} \epsilon_{\mu\tau}^2 \left[2 \sin^2 2\theta_{23} \cos^2 \phi_{\mu\tau} \Delta^2 \cos 2\Delta + \sin^2 \phi_{\mu\tau} \Delta \sin 2\Delta \right]. \quad (17)
\end{aligned}$$

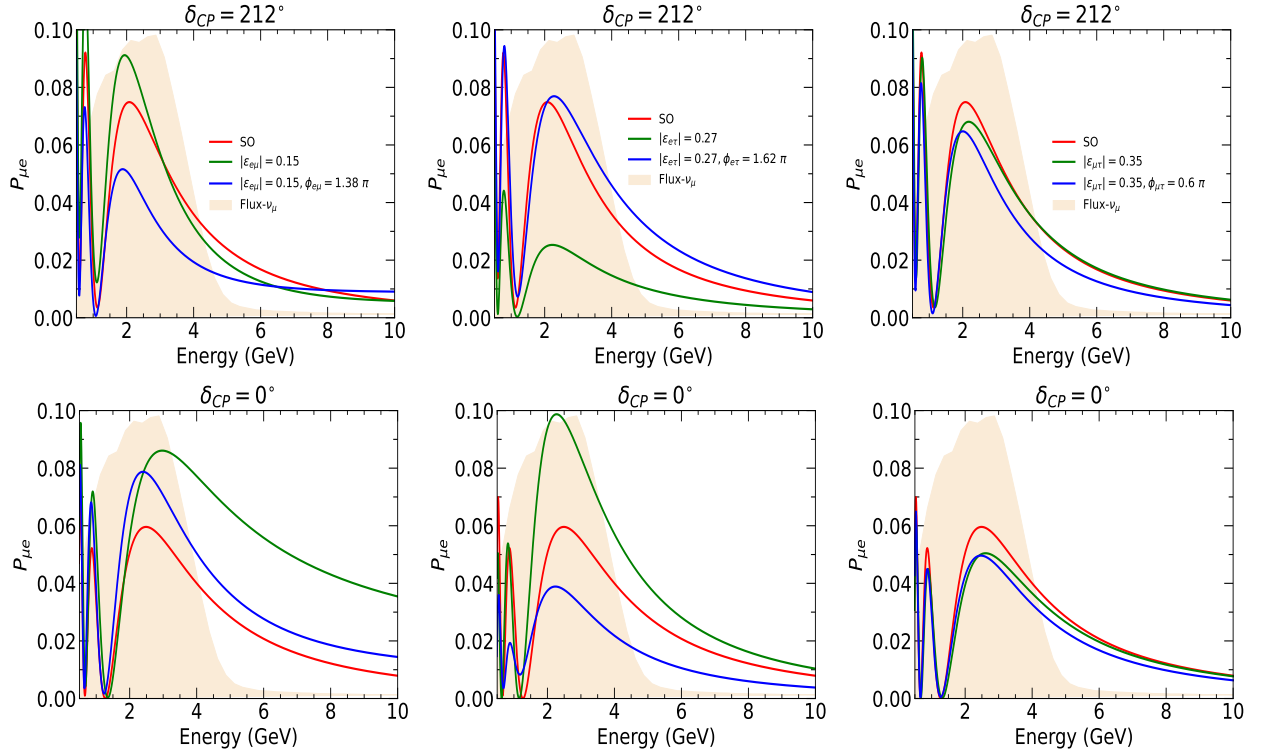


FIG. 1: Upper (lower) row shows the appearance probability as a function of neutrino energy for DUNE experiment with $\delta_{CP} = 212^\circ(0^\circ)$. Left (middle) [right] panel represent the curves with one off-diagonal parameter one at a time, $\epsilon_{e\mu}$ ($\epsilon_{e\tau}$) [$\epsilon_{\mu\tau}$] and their associated phases. Color codes are given in the legend.

From Eq. 17, it is evident that $P_{\mu\mu}$ depends mainly on the NSI parameter $\epsilon_{\mu\tau}$, and is unaffected by $\epsilon_{e\mu}$ and $\epsilon_{e\tau}$. Hence, to investigate the influence of $\epsilon_{e\mu}$ and $\epsilon_{e\tau}$, one should primarily focus on the appearance probability $P_{\mu e}$, while the impact of $\epsilon_{\mu\tau}$ is most effectively studied through the disappearance probability $P_{\mu\mu}$.

² Similar to 15, in the Ref. [61], the expression for $P_{\mu\mu}$ also includes contributions from diagonal NSI terms (such as $\epsilon_{\mu\mu}, \epsilon_{\tau\tau}$). However, Eq. 17 is formulated solely in terms of off-diagonal contributions, keeping $\epsilon_{\mu\mu} = \epsilon_{\tau\tau} = 0$.

Let's first focus on the effect of NSI parameters on the appearance channel. Fig. 1 shows the appearance probability with respect to neutrino energy for different scenarios. Left (middle) panel shows the dependency of $\epsilon_{e\mu}$ ($\epsilon_{e\tau}$) on $P_{\mu e}$ whereas right panel depicts the effect of $\epsilon_{\mu\tau}$. In generating these plots, we use the values of standard oscillation parameters from Table I. For NSI parameters, we take the values from Table II. The specific values of the off-diagonal NSI parameters $\epsilon_{\alpha\beta}$ and their associated phases $\phi_{\alpha\beta}$ considered in Table II are motivated by their potential to resolve the observed tension between the NO ν A and T2K experimental results in the measurement of the leptonic CP-violating phase δ_{CP} and the atmospheric mixing angle θ_{23} [67, 68]. In this analysis, we focus solely on the off-diagonal NSI parameters $\epsilon_{\alpha\beta}$ ($\alpha \neq \beta$), incorporating their associated complex phases $\phi_{\alpha\beta}$ one at a time. This allows us to examine the distinct effects of each off-diagonal NSI term on the oscillation probabilities. We explore three cases for each off diagonal NSI parameters $\epsilon_{\alpha\beta}(\phi_{\alpha\beta})$: (i) the standard oscillation scenario (SO) (ii) NSI with a vanishing complex phase ($\phi_{\alpha\beta} = 0$), and (iii) NSI with a non-zero complex phase ($\phi_{\alpha\beta} \neq 0$). In each panel of Fig. 1, the red curve represents the standard oscillation (SO) scenario, while the green curve corresponds to the case with $\epsilon_{\alpha\beta}$ included. The blue curve illustrates the effect when both $\epsilon_{\alpha\beta}$ and its associated phase $\phi_{\alpha\beta}$ are taken into account. The shaded region corresponds to the DUNE ν_μ neutrino flux in arbitrary units.

The left-most panel of the upper row in Fig. 1 displays the effect of the NSI parameter $\epsilon_{e\mu}$ on the appearance probability when we take $\delta_{CP} = 212^\circ$. From the plot, it is observed that the green curve exhibits a higher amplitude than the red curve. In contrast, the blue curve shows a reduced amplitude compared to the red one. To understand this behavior, we refer to the modified expression for $P_{\mu e}$ in the presence of NSI, considering only $\epsilon_{e\mu}$ and $\phi_{e\mu}$ (i.e., setting $\epsilon_{e\tau} = 0$). The corresponding appearance probability can be expanded as:

$$P(\nu_\mu \rightarrow \nu_e)|_{\epsilon_{e\tau}, \phi_{e\tau}=0} = SO + D1 + E1 + F1 + G1 + J1 + K1 + L1, \quad (18)$$

where

$$\begin{aligned} SO &= x^2 f^2 + 2xyfg \cos(\Delta + \delta_{CP}) + y^2 g^2, & D1 &= 4\hat{A}\epsilon_{e\mu}x f^2 s_{23}^2 \cos(\phi_{e\mu} + \delta_{CP}), \\ E1 &= 4\hat{A}\epsilon_{e\mu}x f g c_{23}^2 \cos(\phi_{e\mu} + \Delta + \delta_{CP}), & F1 &= 4\hat{A}\epsilon_{e\mu}y g^2 c_{23}^2 \cos(\phi_{e\mu}), \\ G1 &= 4\hat{A}\epsilon_{e\mu}y g f s_{23}^2 \cos(\Delta - \phi_{e\mu}), & J1 &= 4\hat{A}^2 g^2 \epsilon_{e\mu}^2 c_{23}^2, \\ K1 &= 4\hat{A}^2 f^2 \epsilon_{e\mu}^2 s_{23}^4, & L1 &= 8\hat{A}^2 f g \epsilon_{e\mu}^2 \sin \theta_{23} \cos \theta_{23} (\cos \theta_{23} \cos \Delta \sin \theta_{23}). \end{aligned} \quad (19)$$

The left and right panels of upper row of Fig. 2 depict $P_{\mu e}$ as a function of neutrino energy for $\epsilon_{e\mu} = 0.15$ with $\phi_{e\mu} = 0$ and 1.38π , respectively. In both cases, we show the individual contributions from each term in Eq. 18. It is evident that D1 and E1 terms dominate the overall modification to the appearance probability. When $\phi_{e\mu} = 0$, the D1 term contributes negatively, while the E1 term gives a positive enhancement in amplitude

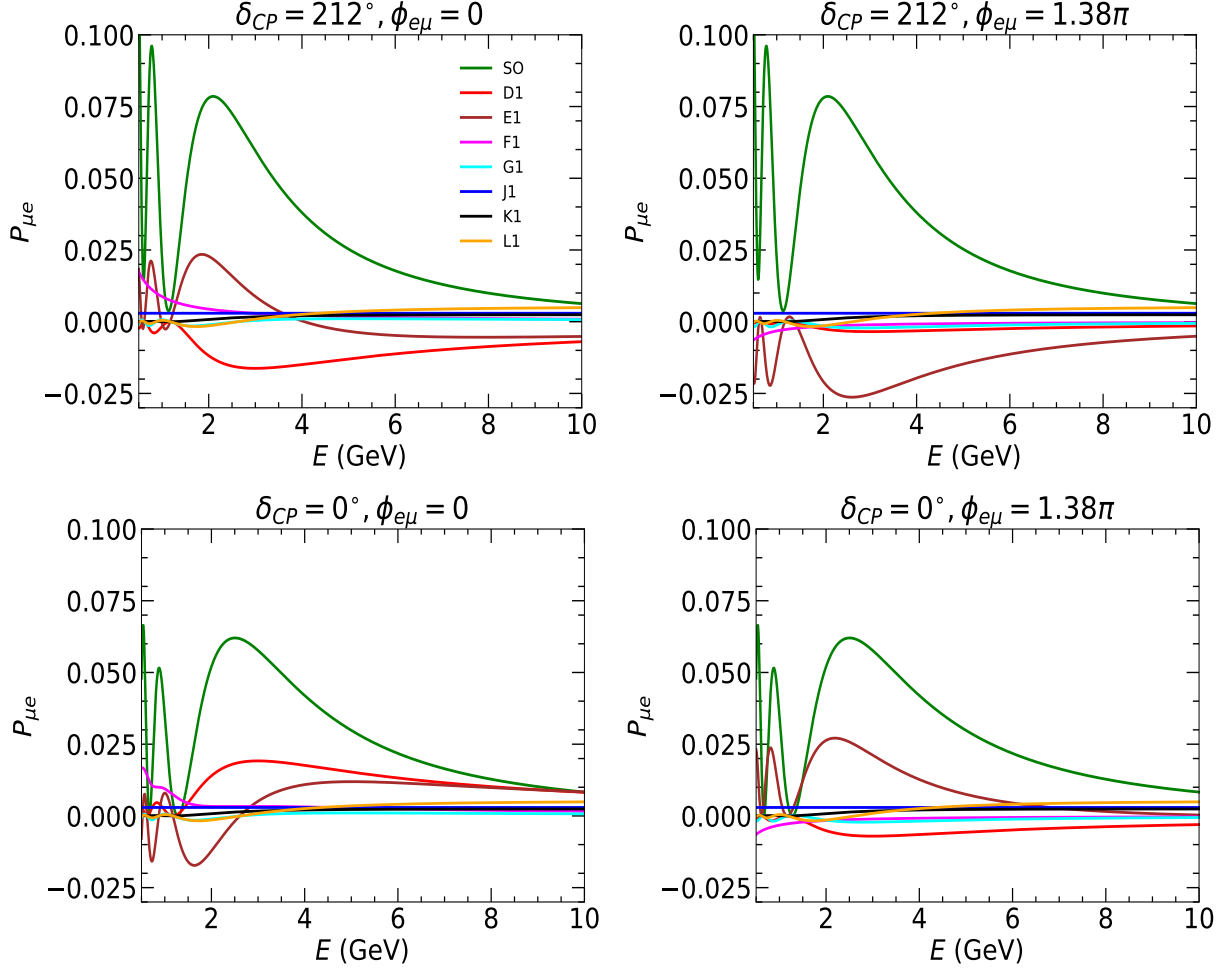


FIG. 2: Upper (lower) row shows the effect of each term containing $\epsilon_{e\mu}$ and $\phi_{e\mu}$ in appearance probability as a function of neutrino energy with $\delta_{CP} = 212^\circ$ (0°). Left (right) panel shows the results with $\phi_{e\mu} = 0$ (1.38π). Color codes are given in the legend. Each term is thoroughly explained within the text.

up to around 4 GeV, followed by a reduction beyond that. Although these contributions act in opposite directions, their combined effect increases the overall amplitude without shifting the oscillation peak, since their maximum and minimum occur at the same energy.

For $\phi_{e\mu} = 1.38\pi$, the behavior changes notably. The E1 term now contributes negatively across the entire energy range, and the D1 term becomes nearly negligible. This change in behavior of E1 term arises due to the cosine dependence in E1: $\cos(\phi_{e\mu} + \Delta + \delta_{CP})$. At $\delta_{CP} = 212^\circ$ and $\phi_{e\mu} = 0$, this term is positive around the oscillation peak. However, for $\phi_{e\mu} = 1.38\pi$, it becomes negative over the full energy spectrum. A similar reasoning applies to the D1 term, which contains $\cos(\phi_{e\mu} + \delta_{CP})$ and thus has minimal contribution at 1.38π . Additionally, in the upper row of the leftmost panel of Fig. 1, the green curve exceeds the red curve only up to about 4 GeV, after which the red curve overtakes. This behavior aligns with the left panel of the upper row of Fig. 2, where the E1 term becomes negative beyond

4 GeV for $\phi_{e\mu} = 0$.

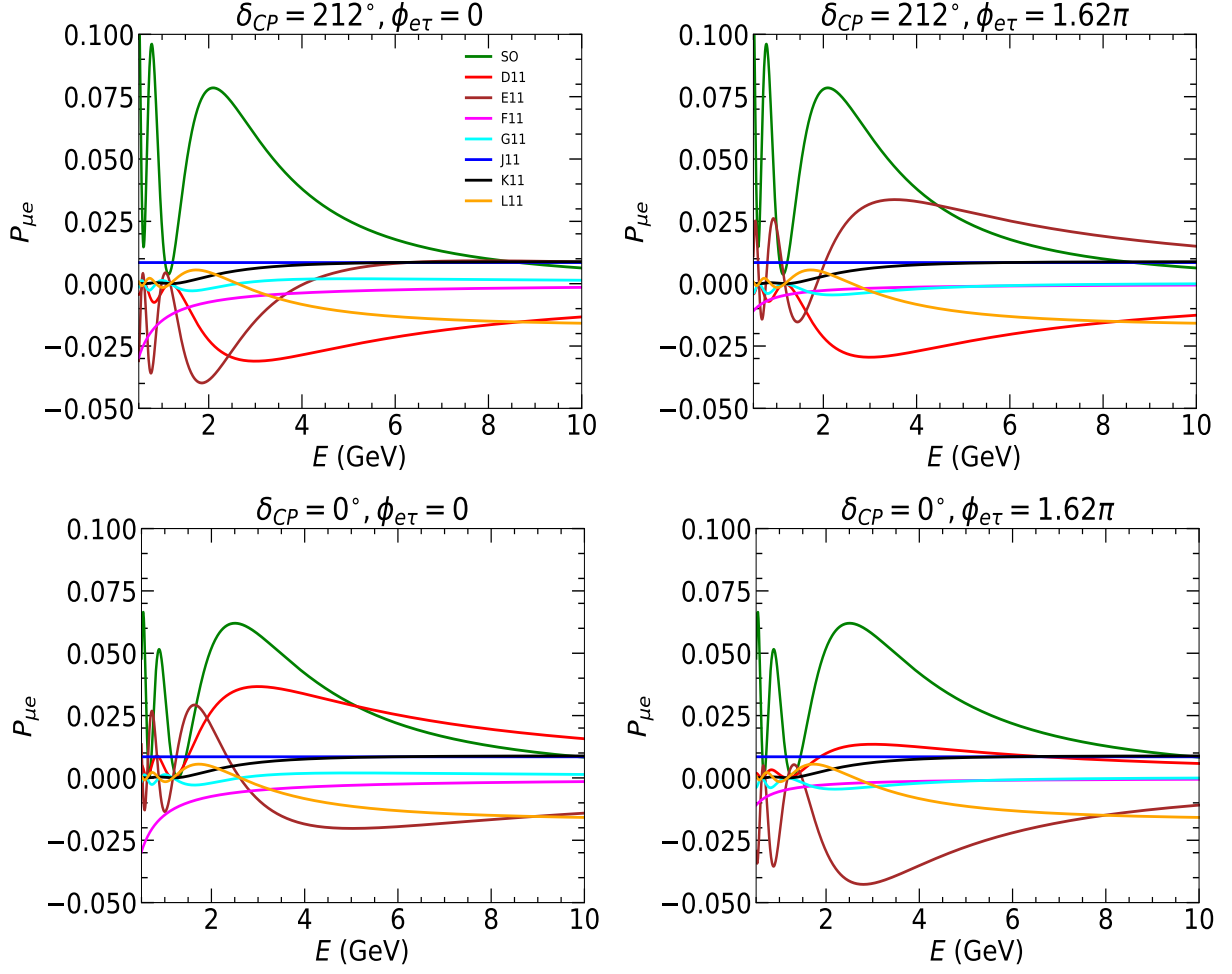


FIG. 3: Upper (lower) row shows the effect of each term containing $\epsilon_{e\tau}$ and $\phi_{e\tau}$ in appearance probability as a function of neutrino energy with $\delta_{CP} = 212^\circ$ (0°). Left (right) panel shows the results with $\phi_{e\tau} = 0$ (1.62π rad). Color codes are given in the legend. For more about each term, see the text.

Unlike the green curve in Fig. 1, the blue curve consistently shows a lower amplitude than the red curve across the full energy range up to 8 GeV. This suppression is directly attributable to the negative E1 contribution shown in the right panel of upper row of Fig. 2, which dominates when $\phi_{e\mu} = 1.38\pi$.

To investigate the combined effect of NSI and the CP-violating phase δ_{CP} on the appearance probability, we consider a CP-conserving scenario with $\delta_{CP} = 0^\circ$, as shown in the lower row in Fig. 1. The color scheme in this panel follows the same convention as the upper row: the red curve corresponds to standard oscillation, the green curve represents the case with only $\epsilon_{e\mu}$, and the blue curve includes both $\epsilon_{e\mu}$ and the phase $\phi_{e\mu}$. From the leftmost plot of the lower row of Fig. 1, it is evident that the red curve lies below both the green and blue

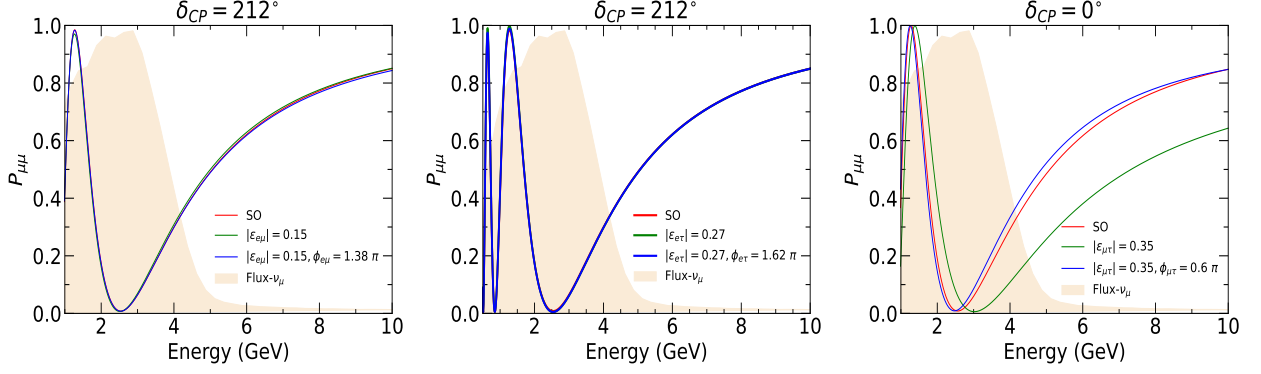


FIG. 4: The disappearance probability as a function of neutrino energy for the DUNE experiment with $\delta_{CP} = 212^\circ$. Left (middle) [right] panel represent the curves with one off-diagonal parameter one at a time, $\epsilon_{e\mu}$ ($\epsilon_{e\tau}$) [$\epsilon_{\mu\tau}$] and their associated phases. Color codes are given in the legend.

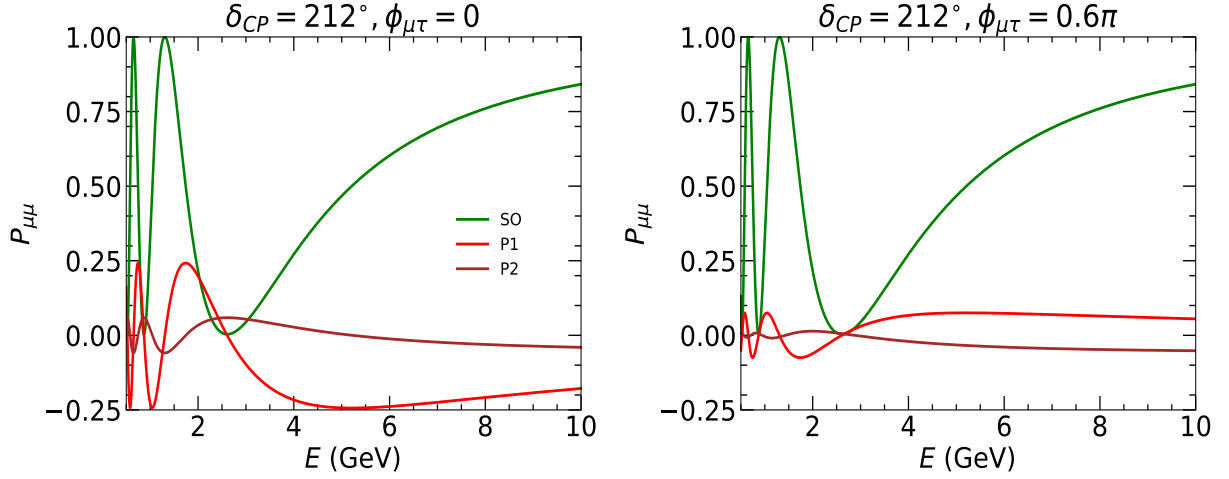


FIG. 5: The effect of each term containing $\epsilon_{\mu\tau}$ and $\phi_{\mu\tau}$ in disappearance probability as a function of neutrino energy with $\delta_{CP} = 212^\circ$. Left (right) panel shows the results with $\phi_{\mu\tau} = 0$ (0.6π rad). Color codes are given in the legend. For more about each term, see the text.

curves across the entire energy range. Between the green and blue curves, the green curve shows a higher amplitude than the blue one.

This behavior is further clarified in the lower panel of Fig. 2, which decomposes the individual contributions to $P_{\mu e}$ under the same parameter settings as the upper panel but with $\delta_{CP} = 0^\circ$. Similar to the upper panels, the D1 and E1 terms are found to contribute most significantly to the overall modification of the appearance probability.

The overall amplitude for the configuration with $\epsilon_{e\mu} = 0.15$ and $\phi_{e\mu} = 0$ is larger than that of the setup with $\epsilon_{e\mu} = 0.15$ and $\phi_{e\mu} = 1.38\pi$; this trend is clearly visible in the lower panel of Fig. 2.

Now we analyze the impact of the NSI parameter $\epsilon_{e\tau}$ on the appearance probability. The middle panel of Fig. 1 illustrates this effect, where the upper row corresponds to $\delta_{CP} = 212^\circ$ and the lower row to $\delta_{CP} = 0^\circ$. The red curve represents the standard oscillation scenario, the green curve shows the probability in the presence of non-zero $\epsilon_{e\tau}$, and the blue curve corresponds to the case with $\epsilon_{e\tau} = 0.27$ and $\phi_{e\tau} = 1.62\pi$. For $\delta_{CP} = 212^\circ$, the green curve has a significantly lower amplitude than the red curve, indicating a suppression in the appearance probability due to the presence of $\epsilon_{e\tau}$. The blue curve, on the other hand, closely follows the red curve, suggesting only a minor effect from the inclusion of the NSI phase in this case.

However, when $\delta_{CP} = 0^\circ$ in Fig. 1, the overall pattern changes. The green curve now shows a much higher amplitude than the red curve, while the blue curve exhibits the lowest amplitude among the three. This change highlights the sensitivity of the appearance probability to both the magnitude and phase of the NSI parameter $\epsilon_{e\tau}$, as well as its strong interplay with the CP-violating phase δ_{CP} .

To understand the behavior of the effect of $\epsilon_{e\tau}$ on $P_{\mu e}$, we split each term of the appearance probability given in eq. 15 as, by taking $\epsilon_{e\tau}$ and $\phi_{e\tau}$ only, keeping $\epsilon_{e\mu} = 0$,

$$P(\nu_\mu \rightarrow \nu_e)|_{\epsilon_{e\mu}, \phi_{e\mu}=0} = SO + D11 + E11 + F11 + G11 + J11 + K11 + L11, \quad (20)$$

where, the expression of SO is given in eq. 18 and the other terms are given as

$$\begin{aligned} D11 &= 4\hat{A}\epsilon_{e\tau}s_{23}c_{23}xf^2\cos(\phi_{e\tau} + \delta_{CP}), & E11 &= -4\hat{A}\epsilon_{e\tau}s_{23}c_{23}xfg\cos(\Delta + \phi_{e\tau} + \delta_{CP}), \\ F11 &= -4\hat{A}\epsilon_{e\tau}s_{23}c_{23}yg^2\cos\phi_{e\tau}, & G11 &= 4\hat{A}\epsilon_{e\tau}s_{23}c_{23}ygf\cos(\Delta - \phi_{e\tau}), \\ J11 &= 4\hat{A}^2g^2\epsilon_{e\tau}^2s_{23}^2c_{23}^2, & K11 &= 4\hat{A}^2f^2\epsilon_{e\tau}^2s_{23}^2c_{23}^2, & L11 &= -8\hat{A}^2fg\epsilon_{e\tau}^2s_{23}^2c_{23}^2\cos\Delta. \end{aligned} \quad (21)$$

Figure 3 presents the energy dependence of the individual terms contributing to the appearance probability. The upper and lower panels correspond to $\delta_{CP} = 212^\circ$ and $\delta_{CP} = 0^\circ$, respectively, while the left and right columns show results for $\phi_{e\tau} = 0$ and $\phi_{e\tau} = 1.62\pi$. In the case of $\delta_{CP} = 212^\circ$, it is evident that the terms D11, E11, and L11 dominate the behavior of $P_{\mu e}$, with the remaining terms contributing negligibly. For $\phi_{e\tau} = 0$, all three dominant terms, D11, E11, and L11 exhibit negative amplitudes throughout the energy range, leading to an overall suppression of the appearance probability compared to the standard oscillation scenario. This observation aligns with the green curve in the middle panel of the upper row in Fig. 1.

When $\phi_{e\tau} = 1.62\pi$, the E11 term becomes positive, while D11 and L11 remain negative. This results in a slight enhancement of the overall amplitude compared to the case with $\phi_{e\tau} = 0$, although the appearance probability is still close to that of standard oscillations, as shown by the blue curve in the corresponding panel of Fig. 1.

For the CP-conserving case with $\delta_{CP} = 0^\circ$, the behavior changes considerably. The lower panel of Fig. 3 reveals that when $\phi_{e\tau} = 0$, D11 and E11 contribute positively, while L11 remains negative. The combined effect of these terms leads to a significantly higher

appearance probability than that of standard oscillations, which is consistent with the green curve in the middle column of lower row of Fig. 1. However, for $\phi_{e\tau} = 1.62\pi$, E11 and L11 contribute large negative amplitudes, while D11 shows positive amplitude. This results in a strong suppression of the overall appearance probability, reflected in the blue curve in the corresponding panel of Fig. 1.

Finally, we examine the influence of $\epsilon_{\mu\tau}$ on the appearance probability. The right-most panels of the upper and lower rows of Fig. 1 illustrate this effect for $\delta_{CP} = 212^\circ$ and $\delta_{CP} = 0^\circ$, respectively. The color scheme remains consistent with the previous panels: the red curve corresponds to standard oscillations, the green curve represents the scenario with non-zero $\epsilon_{\mu\tau}$ and $\phi_{\mu\tau} = 0$, and the blue curve shows the result for $\epsilon_{\mu\tau} = 0.35$ and $\phi_{\mu\tau} = 0.6\pi$. As observed in both CP-violating and CP-conserving cases, the green and blue curves exhibit only slight deviations from the red curve. This indicates that the presence of $\epsilon_{\mu\tau}$ leads to relatively minor modifications in the appearance probability. This behavior is consistent with the analytical expression of $P_{\mu e}$ given in Eq. 15, which shows that $\epsilon_{\mu\tau}$ does not contribute to the probability up to $\mathcal{O}(\epsilon^2)$. However, if the expression is expanded to higher orders, specifically beyond $\mathcal{O}(\epsilon^2)$, subleading terms involving $\epsilon_{\mu\tau}$ may appear. These higher-order contributions can account for the small deviations observed in the rightmost column of Fig. 1.

Now, we explore the impact of NSI parameters on the disappearance probability. According to Eq. 17, the disappearance channel $P_{\mu\mu}$ is primarily influenced by $\epsilon_{\mu\tau}$ and its associated phase $\phi_{\mu\tau}$. Figure 4 illustrates the effects of three different NSI parameters on the disappearance probability separately. The left and middle columns show the effects of $\epsilon_{e\mu}$ and $\epsilon_{e\tau}$, respectively, while the rightmost column presents the impact of $\epsilon_{\mu\tau}$. The color scheme remains consistent throughout: the red curve represents the standard oscillation scenario, the green curve shows the result when $\epsilon_{\alpha\beta}$ is non-zero (with the corresponding phase set to zero), and the blue curve corresponds to the case where both $\epsilon_{\alpha\beta}$ and $\phi_{\alpha\beta}$ are non-zero. The shaded area represents the ν_μ flux for the DUNE experiment in arbitrary units.

From the figure (Fig. 4), it is evident that when either $\epsilon_{e\mu}$ or $\epsilon_{e\tau}$ is present, the green and blue curves show negligible deviations from the standard oscillation (red curve). This observation is consistent with the analytical form of Eq. 17, which shows independent behaviour on these parameters in the disappearance channel. However, the presence of $\epsilon_{\mu\tau}$ and its phase leads to a noticeable change in the disappearance probability. The rightmost column clearly shows a significant deviation of the green curve from the red curve, indicating the strong effect of $\epsilon_{\mu\tau}$ when the phase is set to zero. Interestingly, the blue curve, which includes both $\epsilon_{\mu\tau}$ and $\phi_{\mu\tau}$, mostly overlaps with the red curve. Furthermore, there is an observable shift in the oscillation minimum for the green curve relative to the red and blue curves, highlighting the sensitivity of $P_{\mu\mu}$ to $\epsilon_{\mu\tau}$ in the absence of a complex phase. To

understand the nature, we need to split the modified expression of $P_{\mu\mu}$,

$$P(\nu_\mu \rightarrow \nu_\mu) = SO + P1 + P2, \quad (22)$$

where SO is the first five terms of eq. 17 and

$$\begin{aligned} P1 &= -2\hat{A}\epsilon_{\mu\tau} \cos \phi_{\mu\tau} \left[\sin^3 2\theta_{23} \Delta \sin 2\Delta + 2 \sin 2\theta_{23} \cos^2 2\theta_{23} \sin^2 \Delta \right] \\ P2 &= -2\hat{A}^2 \sin^2 2\theta_{23} \epsilon_{\mu\tau}^2 \left[2 \sin^2 2\theta_{23} \cos^2 \phi_{\mu\tau} \Delta^2 \cos 2\Delta + \sin^2 \phi_{\mu\tau} \Delta \sin 2\Delta \right]. \end{aligned} \quad (23)$$

Figure 5 illustrates the contribution of each term to the disappearance probability. Let us first consider the scenario where $\epsilon_{\mu\tau} = 0.35$ and $\phi_{\mu\tau} = 0$. In this case, the left panel of Fig. 5 shows that the term P1 causes a noticeable shift in the oscillation minimum compared to the standard oscillation. Additionally, beyond the oscillation minimum, the P1 curve exhibits a negative amplitude, leading to an overall suppression of the probability relative to the standard case.

However, when the phase is set to $\phi_{\mu\tau} = 0.6\pi$, both P1 and P2 have a negligible impact on the standard oscillation behavior. As a result, the corresponding blue curve in the rightmost column of Fig. 4 nearly overlaps with the standard oscillation curve, indicating minimal deviation.

B. Analysis based on quantum entanglement measures

In this subsection, we discuss how the off-diagonal NSI parameters influence the entanglement measures: Entanglement of Formation (EOF), Concurrence, and Negativity. Since all three entanglement measures are functions of neutrino oscillation and survival probabilities, the impact of NSI parameters on these quantities is essentially determined by their influence on the oscillation probabilities.

Figure 6 illustrates how the NSI parameter, $\epsilon_{e\mu}$ affects EOF, Concurrence, and Negativity. In each panel, the red curve corresponds to the standard oscillation scenario with no NSI present. The green curve shows the effect of a non-zero real part, specifically $\epsilon_{e\mu} = 0.15$ with the associated phase $\phi_{e\mu} = 0$. The blue curve includes both the real and imaginary components of $\epsilon_{e\mu}$, i.e., the full complex parameter. The shaded region represents the ν_μ flux in arbitrary units. The left, middle, and right panels of Fig. 6 respectively depict the variation of EOF, Concurrence, and Negativity due to the presence of $\epsilon_{e\mu}$. For these plots, the standard oscillation parameters are taken from Table I, while the NSI values are from Table II. Upper row of Fig. 6 shows the result when $\delta_{CP} = 212^\circ$ whereas lower row represents the result with $\delta_{CP} = 0^\circ$.

To understand the influence of the $\epsilon_{e\mu}$ parameter on the Entanglement of Formation (EOF), we refer to the leftmost panel of the upper row in Fig. 6. Around the DUNE flux oscillation peak, approximately at 2.5 GeV, a clear deviation of the blue curve from the

standard oscillation curve (red) is observed. When both the real and imaginary components of $\epsilon_{e\mu}$ are included, the EOF value decreases at this oscillation peak. In contrast, if only the real part of $\epsilon_{e\mu}$ is considered, there is a slight enhancement in the EOF amplitude at the same energy compared to the standard case. This behavior continues consistently up to around 5 GeV, beyond which all three curves converge and exhibit negligible differences. In the lower row of the leftmost panel, with $\delta_{CP} = 0^\circ$, the EOF displays a different trend. Here, the green curve diverges significantly from both the red and blue curves, particularly beyond 4 GeV, where the difference between the green and red curves becomes more pronounced.

To explain the nature of both the panels, we need to see the numerical expression. The expression of EOF in terms of oscillation probabilities are given in Eq. 10. In this study, we mainly focus on the accelerator-based long-baseline experiment DUNE. For the DUNE experimental setup, the experiment is sensitive to measure the appearance and disappearance probabilities of muon electron neutrinos. Thus, we need to express Eq. 10 in terms of $P_{\mu e}$ and $P_{\mu\mu}$. The modified form of the equation 10 (considering ν_μ as initial neutrino flavor) in terms of $P_{\mu e}$ and $P_{\mu\mu}$ is given by:

$$EOF = -\frac{1}{2} \left[P_{\mu e} \log_2 P_{\mu e} + P_{\mu\mu} \log_2 P_{\mu\mu} + (1 - P_{\mu e} - P_{\mu\mu}) \log_2 (1 - P_{\mu e} - P_{\mu\mu}) + (1 - P_{\mu e}) \times \log_2 (1 - P_{\mu e}) + (1 - P_{\mu\mu}) \log_2 (1 - P_{\mu\mu}) + (P_{\mu\mu} + P_{\mu e}) \log_2 (P_{\mu\mu} + P_{\mu e}) \right]. \quad (24)$$

From Eq. 24, it is evident that the EOF depends equally on both the appearance probability $P_{\mu e}$ and the disappearance probability $P_{\mu\mu}$. However, as shown in Eq. 17 and Fig. 4, the influence of the NSI parameter $\epsilon_{e\mu}$ on the disappearance channel is minimal. Therefore, the behavior of EOF is primarily governed by the appearance probability in presence of the NSI parameter $\epsilon_{e\mu}$, as described in Eq. 15 and illustrated in Fig. 1.

Both the analytical expression and the plots indicate that the behavior of $P_{\mu e}$ in the presence of $\epsilon_{e\mu}$ closely mirrors the pattern observed in the leftmost column of Fig. 6. For instance, at $\delta_{CP} = 212^\circ$, near the oscillation peak, the blue curve lies below the red (standard) curve, while the green curve exhibits a higher amplitude, matching the pattern seen in the left panel of the upper row of Fig. 1. Similarly, for $\delta_{CP} = 0^\circ$, the behavior in the lower row of the leftmost panel in Fig. 6 closely resembles that of the corresponding panel in Fig. 1. From this analysis, it becomes clear that the impact of $\epsilon_{e\mu}$ on the EOF is predominantly driven by its effect on the appearance channel.

Next, we turn our attention to understanding how $\epsilon_{e\mu}$ influences the other two entanglement measures: Concurrence and Negativity. The simplified form of Concurrence (Eq. 12) in terms of electron neutrino appearance and muon neutrino disappearance probabilities as,

$$C^\mu = 2\sqrt{P_{\mu\mu}(1 - P_{\mu\mu} - P_{\mu e}) + P_{\mu e}(1 - P_{\mu e})}. \quad (25)$$

Similarly, the expression of Negativity in terms of $P_{\mu e}$ and $P_{\mu\mu}$ as:

$$N^\mu = [\sqrt{P_{\mu e}}\sqrt{1 - P_{\mu e}}\sqrt{1 - P_{\mu\mu}}\sqrt{P_{\mu\mu}}\sqrt{P_{\mu e} + P_{\mu\mu}}\sqrt{1 - P_{\mu e} - P_{\mu\mu}}]^\frac{1}{3}. \quad (26)$$

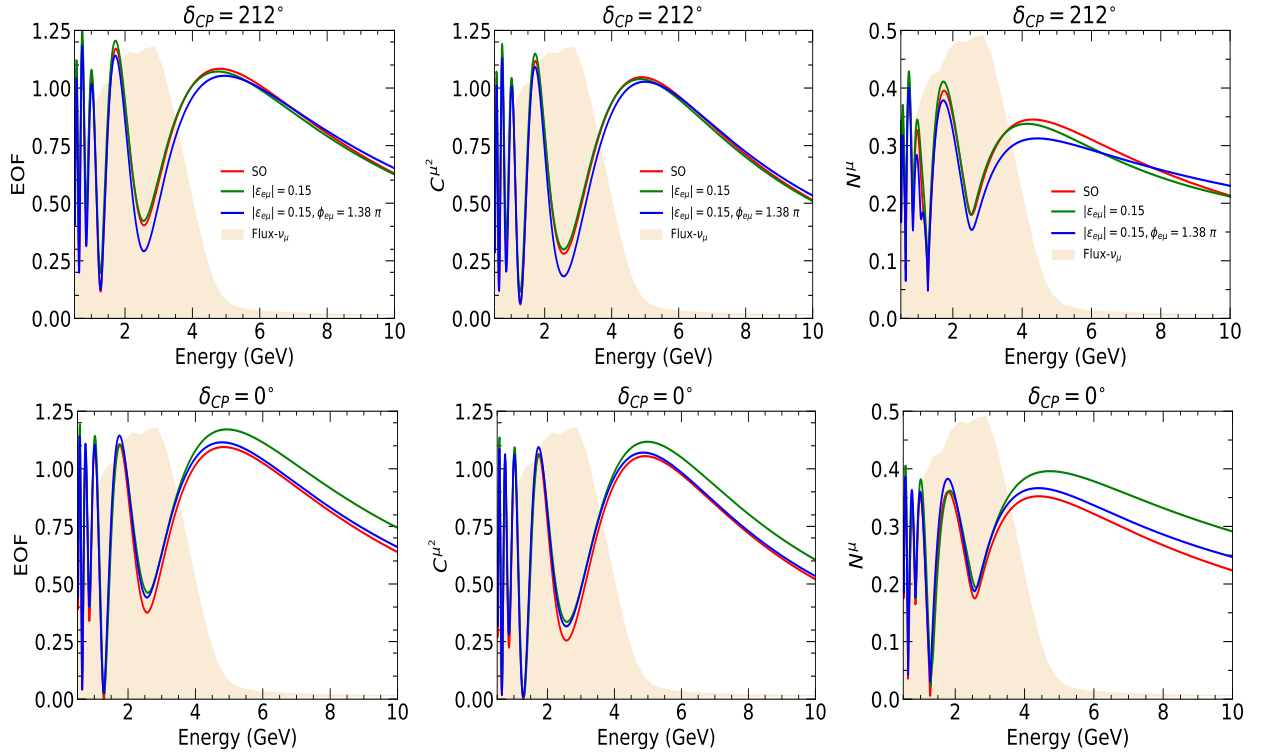


FIG. 6: Upper (lower) row shows the NSI parameter ($\epsilon_{e\mu}$) dependency on EOF(left), Concurrence(middle) and Negativity(right) for DUNE experiment with $\delta_{CP} = 212^\circ$ (0°).

If we examine the middle and right-most columns of Fig. 6, it becomes clear that both Concurrence and Negativity exhibit a similar pattern to that of the EOF in the presence of the $\epsilon_{e\mu}$ parameter. This similarity suggests that their behavior, like EOF, can be primarily attributed to the modifications in the appearance channel alone.

In conclusion, Fig. 6 demonstrates that the presence of the off-diagonal NSI parameter $\epsilon_{e\mu}$ leads to a noticeable deviation in the behavior of all three entanglement measures compared to the standard scenario. This deviation becomes more pronounced when δ_{CP} corresponds to a CP-conserving value.

Figure 7 illustrates the impact of the NSI parameter $\epsilon_{e\tau}$ on the three entanglement measures: EOF, Concurrence, and Negativity. The color scheme remains consistent with the previous figure; red denotes the standard oscillation scenario, green corresponds to a non-zero real value of $\epsilon_{e\tau}$ with phase $\phi_{e\tau} = 0$ rad, and blue represents the case where both real and imaginary parts of $\epsilon_{e\tau}$, along with its associated phase $\phi_{e\tau}$, are considered. The shaded area corresponds to the DUNE ν_μ neutrino flux in arbitrary units.

In the upper row with $\delta_{CP} = 212^\circ$, all three measures show that the green curve lies below both the red and blue curves at the oscillation peak. At higher neutrino energies, the three curves converge for EOF and Concurrence, indicating negligible differences. However, in the case of Negativity, the curves remain distinct even at higher energies. For $\delta_{CP} = 0^\circ$, shown in the lower row, the blue curve lies below the red and green curves at the oscillation maximum

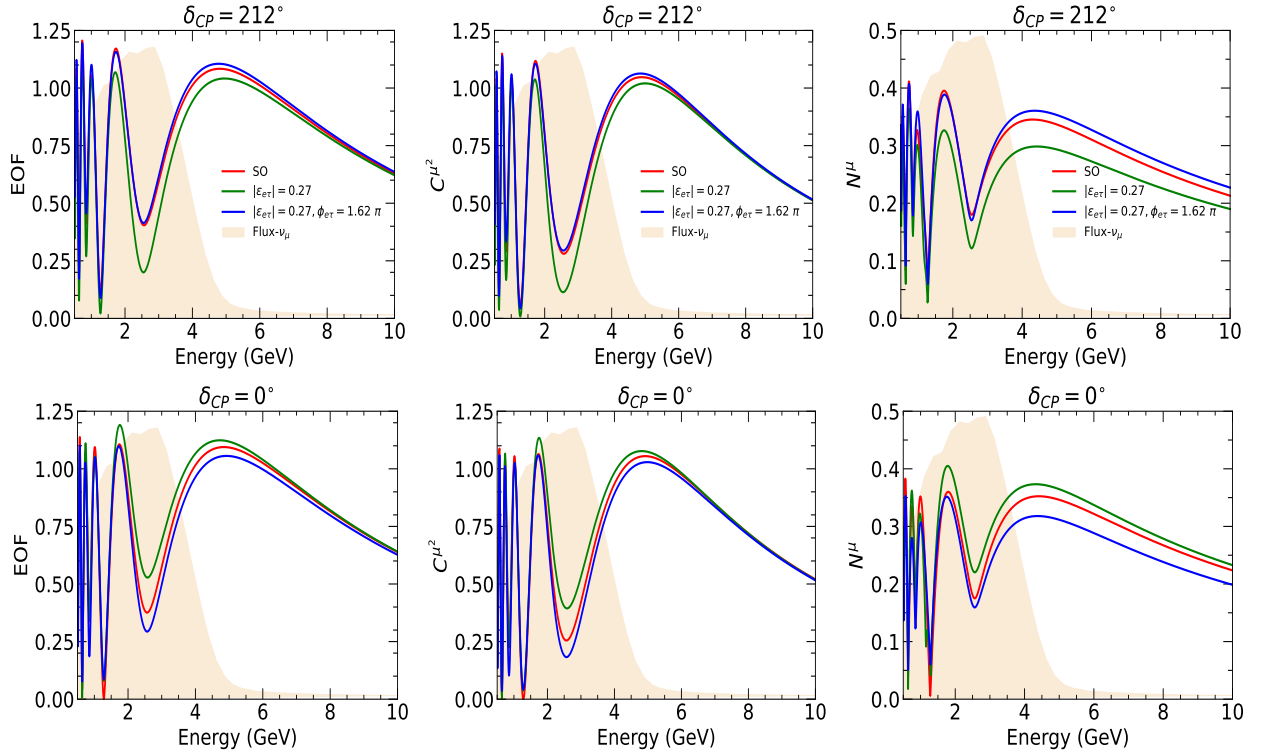


FIG. 7: Upper (lower) row shows the NSI parameter ($\epsilon_{e\tau}$) dependency on EOF(left), Concurrence(middle) and Negativity(right) for DUNE experiment with $\delta_{CP} = 212^\circ$ (0°).

across all three entanglement measures. As the energy increases, the curves tend to overlap for EOF and Concurrence, while they remain clearly separated for Negativity. The overall behavior observed in Fig. 7 can be attributed solely to the effect of $\epsilon_{e\tau}$ on the appearance probability, as the disappearance probability $P_{\mu\mu}$ is unaffected by this parameter.

In Fig. 8, all three entanglement measures; EOF, Concurrence, and Negativity exhibit a consistent pattern across the energy spectrum for the NSI scenario involving $\epsilon_{\mu\tau}$. In contrast to the cases with $\epsilon_{e\mu}$ and $\epsilon_{e\tau}$, a noticeable shift is observed in the curves for the scenario with $\phi_{\mu\tau} = 0$, particularly around the oscillation peak. This deviation highlights the significant role played by the phase $\phi_{\mu\tau}$ in shaping the entanglement behavior. As evident from Eqs. 15 and 17, the appearance probability $P_{\mu e}$ does not depend on $\epsilon_{\mu\tau}$ at leading order, whereas the disappearance probability $P_{\mu\mu}$ is strongly influenced by this parameter. Consequently, the behavior of EOF, Concurrence, and Negativity closely follows the trends shown in the rightmost panel of Fig. 4.

In summary, for long-baseline accelerator neutrino experiments, the influence of off-diagonal NSI parameters on entanglement measures is primarily governed by their impact on the appearance and disappearance channels. Specifically, the parameters $\epsilon_{e\mu}$ and $\epsilon_{e\tau}$ predominantly affect the appearance probability $P_{\mu e}$, while $\epsilon_{\mu\tau}$ modifies the disappearance probability $P_{\mu\mu}$.

Additionally, similar patterns in the entanglement measures; EOF, Concurrence, and

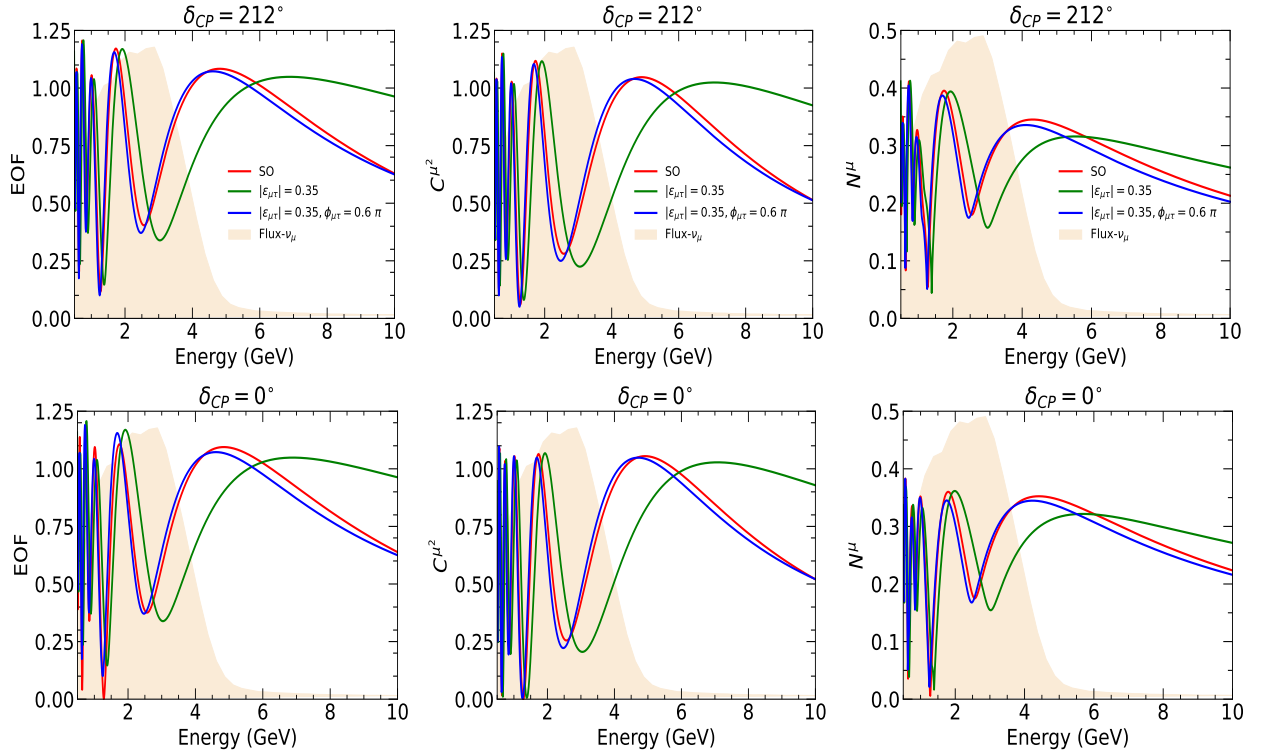


FIG. 8: Upper (lower) row shows the NSI parameter ($\epsilon_{\mu\tau}$) dependency on EOF(left), Concurrence(middle) and Negativity(right) for DUNE experiment with $\delta_{CP} = 212^\circ$ (0°).

Negativity are observed in future long-baseline experiments such as P2SO when these off-diagonal NSI parameters are introduced.

VI. CONCLUSION

In this study, we investigated the impact of off-diagonal non-standard interaction (NSI) parameters on quantum entanglement within the three-flavor neutrino oscillation framework. By reformulating three commonly used entanglement measures; Entanglement of Formation (EOF), Concurrence, and Negativity in terms of oscillation probabilities, we analyzed how quantum correlations are modified by the presence of the off-diagonal NSI parameters $\epsilon_{e\mu}$, $\epsilon_{e\tau}$, and $\epsilon_{\mu\tau}$, including the influence of their complex phases.

Focusing on the DUNE experimental setup, we studied how both the magnitude and phase of these parameters affect the energy-dependent behavior of the entanglement measures. Our findings indicate that NSI effects are most prominent at lower neutrino energies, specifically at the oscillation maximum position. Among the three measures, Negativity consistently shows the most pronounced sensitivity to NSI, clearly distinguishing scenarios with non-zero phases from standard oscillations, even at higher energies. Moreover, we found that the entanglement behavior is predominantly governed by the oscillation (or survival)

probabilities: the appearance channel plays the dominant role when $\epsilon_{e\mu}$ or $\epsilon_{e\tau}$ is considered individually, while the disappearance channel becomes central in the case of $\epsilon_{\mu\tau}$.

We also extended our analysis to the P2SO experiment and found that its results closely mirror those of DUNE, with slightly enhanced NSI effects attributable to the longer baseline of P2SO. This similarity indicates that both experiments exhibit comparable behavior in response to off-diagonal NSI parameters. Consequently, it can be inferred that other long-baseline neutrino experiments are likely to show similar trends in their entanglement behavior.

VII. ACKNOWLEDGEMENTS

LK thanks the Ministry of Education (MoE) for financial support and the Indian Institute of Technology Jodhpur for providing necessary research facilities. PP wants to thank Prime Minister's Research Fellows (PMRF) scheme for its financial support. We gratefully acknowledge the use of CMSD HPC facility of University of Hyderabad to carry out the computational works.

-
- [1] Y. Fukuda *et al.* [Super-Kamiokande Collaboration], Phys. Rev. Lett. **81**, 1562–1567 (1998).
 - [2] Q. R. Ahmad *et al.* [SNO Collaboration], Phys. Rev. Lett. **89** (2002), 10.1103/physrevlett.89.011301.
 - [3] K. Abe *et al.* [T2K Collaboration], Eur. Phys. J. C **83** (2023), 10.1140/epjc/s10052-023-11819-x.
 - [4] M. Acero *et al.* [NOvA Collaboration], Phys. Rev. D **106** (2022), 10.1103/physrevd.106.032004.
 - [5] B. Abi *et al.* [DUNE Collaboration], JINST **15**, T08008 (2020), arXiv:2002.02967 [physics.ins-det].
 - [6] J. collaboration *et al.*, Prog. Part. Nucl. Phys. **123**, 103927 (2022).
 - [7] B. Abi *et al.*, Eur. Phys. J. C **81** (2021), 10.1140/epjc/s10052-021-09007-w.
 - [8] R. Majhi, D. K. Singha, M. Ghosh, and R. Mohanta, Phys. Rev. D **107** (2023), 10.1103/physrevd.107.075036.
 - [9] R. Mohanta, in *Particle Physics and Cosmology in the Himalayas* (2025) arXiv:2503.12985 [hep-ph].
 - [10] P. Panda and R. Mohanta, (2024), arXiv:2412.05213 [hep-ph].
 - [11] P. Panda, D. K. Singha, M. Ghosh, and R. Mohanta, Eur. Phys. J. C **85**, 67 (2025), arXiv:2403.09105 [hep-ph].
 - [12] S. K. Pusty, R. Majhi, D. K. Singha, M. Ghosh, and R. Mohanta, (2024), arXiv:2410.23014 [hep-ph].

- [13] C. Bera, K. N. Deepthi, and R. Mohanta, *JHEP* **06**, 179 (2025), arXiv:2501.14383 [hep-ph].
- [14] D. K. Singha, R. Majhi, L. Panda, M. Ghosh, and R. Mohanta, *Phys. Rev. D* **109**, 095038 (2024), arXiv:2308.10789 [hep-ph].
- [15] T. Ohlsson, *Rept. Prog. Phys.* **76**, 044201 (2013), arXiv:1209.2710 [hep-ph].
- [16] O. G. Miranda and H. Nunokawa, *New J. Phys.* **17**, 095002 (2015), arXiv:1505.06254 [hep-ph].
- [17] Y. Farzan and M. Tortola, *Front. in Phys.* **6**, 10 (2018), arXiv:1710.09360 [hep-ph].
- [18] C. Biggio, M. Blennow, and E. Fernández-Martínez, *JHEP* **2009**, 090–090 (2009).
- [19] K. N. Deepthi, S. C, and R. Mohanta, *New J. Phys.* **17**, 023035 (2015), arXiv:1409.2343 [hep-ph].
- [20] S. Fukasawa, M. Ghosh, and O. Yasuda, *Nucl. Phys. B* **918**, 337 (2017), arXiv:1607.03758 [hep-ph].
- [21] M. Masud, A. Chatterjee, and P. Mehta, *J. Phys. G* **43**, 095005 (2016), arXiv:1510.08261 [hep-ph].
- [22] A. de Gouvêa and K. J. Kelly, *Nucl. Phys. B* **908**, 318 (2016), arXiv:1511.05562 [hep-ph].
- [23] K. Deepthi, S. Goswami, and N. Nath, *Nucl. Phys. B* **936**, 91–105 (2018).
- [24] M. Blennow, P. Coloma, E. Fernandez-Martinez, J. Hernandez-Garcia, and J. Lopez-Pavon, *JHEP* **2017** (2017), 10.1007/jhep04(2017)153.
- [25] S. K. Agarwalla, S. S. Chatterjee, and A. Palazzo, *Phys. Lett. B* **762**, 64–71 (2016).
- [26] M. Masud and P. Mehta, *Phys. Rev. D* **94** (2016), 10.1103/physrevd.94.053007.
- [27] P. Coloma and T. Schwetz, *Phys. Rev. D* **95** (2017), 10.1103/physrevd.95.079903.
- [28] J. Liao, D. Marfatia, and K. Whisnant, *Phys. Rev. D* **93** (2016), 10.1103/physrevd.93.093016.
- [29] P. Coloma, *JHEP* **2016** (2016), 10.1007/jhep03(2016)016.
- [30] A. K. Alok, S. Banerjee, and S. Uma Sankar, *Nucl. Phys. B* **909**, 65–72 (2016).
- [31] S. Banerjee, A. K. Alok, R. Srikanth, and B. C. Hiesmayr, *Eur. Phys. J. C* **75**, 1 (2015).
- [32] J. Formaggio, D. Kaiser, M. Murskyj, and T. Weiss, *Phys. Rev. Lett.* **117** (2016), 10.1103/physrevlett.117.050402.
- [33] Q. Fu and X. Chen, *Eur. Phys. J. C* **77** (2017), 10.1140/epjc/s10052-017-5371-y.
- [34] J. Naikoo, A. K. Alok, S. Banerjee, and S. U. Sankar, *Phys. Rev. D* **99** (2019), 10.1103/physrevd.99.095001.
- [35] J. Naikoo, A. K. Alok, S. Banerjee, S. Uma Sankar, G. Guarnieri, C. Schultze, and B. C. Hiesmayr, *Nucl. Phys. B* **951**, 114872 (2020).
- [36] S. Shafaq and P. Mehta, *J. Phys. G* **48**, 085002 (2021).
- [37] T. Sarkar and K. Dixit, *Eur. Phys. J. C* **81** (2021), 10.1140/epjc/s10052-021-08874-7.
- [38] M. Blasone, F. Illuminati, L. Petruzzello, and L. Smaldone, *Phys. Rev. A* **108**, 032210 (2023), arXiv:2111.09979 [quant-ph].
- [39] D. S. Chattopadhyay and A. Dighe, *Phys. Rev. D* **108**, 112013 (2023), arXiv:2304.02475 [hep-ph].

- [40] L. Konwar, J. Vardani, and B. Yadav, *Eur. Phys. J. C* **84** (2024), 10.1140/epjc/s10052-024-13370-9.
- [41] K. Dixit, S. S. Haque, and S. Razzaque, *Eur. Phys. J. C* **84** (2024), 10.1140/epjc/s10052-024-12620-0.
- [42] S. Bouri, A. K. Jha, and S. Banerjee, (2024), arXiv:2405.13114 [hep-ph].
- [43] R. Banerjee, P. Panda, R. Mohanta, and S. Patra, (2024), arXiv:2410.05727 [hep-ph].
- [44] L. Konwar and B. Yadav, *J. Phys. G* **52**, 045001 (2025), arXiv:2411.14234 [hep-ph].
- [45] L. Konwar, *Journal of Subatomic Particles and Cosmology* , 100065 (2025).
- [46] M. Blasone, F. Dell’Anno, S. De Siena, and F. Illuminati, *EPL* **85**, 50002 (2009).
- [47] M. Blasone, F. Dell’Anno, S. D. Siena, and F. Illuminati, *Journal of Physics: Conference Series* **237**, 012007 (2010).
- [48] M. Blasone, S. De Siena, and C. Matrella, *Eur. Phys. J. C* **81** (2021), 10.1140/epjc/s10052-021-09471-4.
- [49] A. Kumar Jha, S. Mukherjee, and B. A. Bambah, *Mod. Phys. Lett. A* **36**, 2150056 (2021), arXiv:2004.14853 [hep-ph].
- [50] L. Konwar and B. Yadav, *Nucl. Phys. B* **1002**, 116544 (2024).
- [51] R. Horodecki, P. Horodecki, M. Horodecki, and K. Horodecki, *Rev. Mod. Phys.* **81**, 865–942 (2009).
- [52] M. Blasone, F. Dell’Anno, S. De Siena, M. Di Mauro, and F. Illuminati, *Phys. Rev. D* **77** (2008), 10.1103/physrevd.77.096002.
- [53] C. H. Bennett, D. P. DiVincenzo, J. A. Smolin, and W. K. Wootters, *Phys. Rev. A* **54**, 3824 (1996), arXiv:quant-ph/9604024.
- [54] Y. Guo and L. Zhang, *Phys. Rev. A* **101**, 032301 (2020).
- [55] S. Hill and W. K. Wootters, *Phys. Rev. Lett.* **78**, 5022 (1997), arXiv:quant-ph/9703041.
- [56] W. K. Wootters, *Phys. Rev. Lett.* **80**, 2245 (1998), arXiv:quant-ph/9709029.
- [57] Y. Guo and G. Gour, *Phys. Rev. A* **99**, 042305 (2019).
- [58] A. Peres, *Phys. Rev. Lett.* **77**, 1413 (1996), arXiv:quant-ph/9604005.
- [59] G. Vidal and R. F. Werner, *Phys. Rev. A* **65**, 032314 (2002), arXiv:quant-ph/0102117.
- [60] C. Sabín and G. García-Alcaine, *Eur. Phys. J. C* **48**, 435 (2008).
- [61] J. Liao, D. Marfatia, and K. Whisnant, *JHEP* **01**, 071 (2017), arXiv:1612.01443 [hep-ph].
- [62] L.-J. Li, F. Ming, X.-K. Song, L. Ye, and D. Wang, *Eur. Phys. J. C* **81**, 728 (2021).
- [63] B. Abi *et al.* (DUNE), (2021), arXiv:2103.04797 [hep-ex].
- [64] P. Huber, M. Lindner, and W. Winter, *Comput. Phys. Commun.* **167**, 195 (2005), arXiv:hep-ph/0407333.
- [65] P. Huber, J. Kopp, M. Lindner, M. Rolinec, and W. Winter, *Comput. Phys. Commun.* **177**, 432 (2007), arXiv:hep-ph/0701187.
- [66] I. Esteban, M. C. Gonzalez-Garcia, M. Maltoni, I. Martinez-Soler, J. P. Pinheiro, and T. Schwetz, *JHEP* **2024** (2024), 10.1007/jhep12(2024)216.

- [67] S. S. Chatterjee and A. Palazzo, Phys. Rev. Lett. **126**, 051802 (2021), arXiv:2008.04161 [hep-ph].
- [68] P. B. Denton, J. Gehrlein, and R. Pestes, Phys. Rev. Lett. **126**, 051801 (2021), arXiv:2008.01110 [hep-ph].
- [69] I. Esteban, M. C. Gonzalez-Garcia, M. Maltoni, T. Schwetz, and A. Zhou, JHEP **09**, 178 (2020), arXiv:2007.14792 [hep-ph].